Chapter 7

Expansion and developmental patterning of human PSC-derived cardiovascular progenitors

Matthew J Birket[1], Marcelo C Ribeiro[1], Arie Verkerk[2], Dorien Ward[1], Ana Rita Leitoguinho[1], Sabine den Hartogh[1], Milena Bellin[1], Valeria V Orlova[1], Harsha D Devalla[1], Verena Schwach[1], Robert Passier[1], Christine L Mummery[1]

[1] Leiden University Medical Center, Leiden, The Netherlands.

[2] Amsterdam Medical Center, Amsterdam, The Netherlands.

Nature Biotechnology 2015 33(9):1–12

Abstract

The inability of multipotent cardiovascular progenitor cells (CPCs) to undergo more than a few divisions in culture has precluded stable expansion of precursors of (human) cardiomyocytes and vascular cells. This contrasts with neural progenitors, which can be expanded robustly and are a renewable source of their derivatives. Here, we used human pluripotent stem cells (hPSCs) in which CPCs are genetically marked to show that regulated MYC expression enables their robust expansion through IGF-1 and hedgehog signalling. These CPCs can be patterned with morphogens, recreating features of heart field assignment, and controllably differentiated to relatively pure populations of pacemaker-like or "working" ventricular-like cardiomyocytes with strikingly different physiological characteristics. The cells are clonogenic and can be expanded over 40 population doublings yet still be directed to differentiate to cardiomyocytes as well as vascular cells. Together, this tractable model reveals the potential of hPSC-derived CPCs for precisely recreating elements of heart development in vitro.

Introduction

Human pluripotent stem cells (hPSCs) can recapitulate aspects of development in vitro and produce cell types not routinely available from primary tissue. This has already proven useful in modeling disease, screening compound libraries to identify drug targets and developing cell therapies [1–3]. The heart is of particular relevance because of its vital function and inaccessibility. Differentiation of hPSCs to cardiomyocytes and vascular cells can contribute to understanding the nature of congenital defects in development and disease and in safety pharmacology, as the heart is a crucial target of toxicity [4]. The availability of expandable hPSC-derived multipotent CPCs with the ability to form cardiomyocytes and vascular cells in culture could advance all of these areas by providing renewable precursors without the need to return to the hPSC source. This goal has been challenging because the culture requirements of CPCs are uncertain and their molecular identity is poorly defined [5].

In heart development, CPC populations arise within bilateral cardiogenic areas of mesoderm. Following prior lineage segregation, one CPC population, called the first heart field (FHF), forms the myocardium of the linear heart tube, and the remaining pool of undifferentiated CPCs, called the second heart field (SHF), are added later, providing further cardiomyocytes, smooth muscle and endothelial cells to the developing heart [6]. The genes ISL1 and NKX2-5 (the vertebrate homolog to tinman), which encode homeobox transcription factors, are two of the earliest genes identifying CPCs and may be expressed at least transiently in the majority of these cells [7–9]. Both have been used to isolate multipotent CPCs from embryonic or neonatal hearts and hPSCs, and the potential of these cells for differentiation has been demonstrated in short-term experiments [10–12]. However, the difference between the isolated populations in these respective studies is unclear, and heterogeneity in clonal experiments suggests that there is a need for additional markers and better methods for robustly maintaining discrete populations at different stages of commitment. Expression of Nkx2-5 in mice, for example, is present in the majority of CPCs destined to form 'working' myocardium but is thought to be absent in the SHF lineage destined for the sinoatrial node (SAN) [13]. These SAN progenitors, however, express Isl1 and may also express Tbx18, which encodes a T-box transcription factor14. Conversely, in mice, the FHF CPC population, which gives rise mainly to primitive left ventricular progenitors, may be uniquely marked by early Hcn4 expression [15,16]. Hcn4 is expressed later and then maintained in the $Isl1^{+}Nkx2\text{-}5^{-}Tbx18^{+}$ SHF-CPC–derived SAN. These important commitment steps and their regulatory mechanisms are not resolved in the hPSC model. Generating pure populations of pacemaker cells is crucial for modeling sinus node dysfunction and could be useful in the future development of biological pacemakers; pure populations of ventricular or atrial working myocardial cells would similarly benefit other applications.

The practical challenge for more effectively directing cardiac progression from hPSCs is to slow the otherwise rapid and uncontrolled transition from the appearance of CPCs, marked by increasing expression of platelet-derived growth factor receptor-α (PDGFR-α)[17], to their differentiation, predominantly to cardiomyocytes of heterogeneous identity. Here, taking advantage of $NKX2\text{-}5^{eGFP/w}$ human embryonic stem cells (hESCs) in which the emergence of $NKX2\text{-}5^{+}$ cells can be followed by eGFP expression, we report a solution through

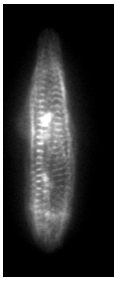

regulated MYC expression. This enables the expansion of primitive pre–NKX2-5$^+$ CPCs, their patterning through regulation of fibroblast growth factor (FGF) and bone morphogenetic protein (BMP) signaling and their directed differentiation to NKX2-5–eGFP$^+$ working ventricular-like cells, NKX2-5–eGFP$^-$ pacemaker-like cells and endothelial and, later, smooth muscle cells, mimicking the cardiac developmental program.

Results

Regulated MYC expression restrains cardiac differentiation

A doxycycline-inducible MYC transgene (Tet-On-MYC) was introduced into an NKX2-5$^{eGFP/w}$ hESC line to allow MYC expression to be controlled during differentiation. In NKX2-5e$^{GFP/w}$ Tet-On-MYC hESCs and day 5 embryoid bodies (EBs) derived from them, MYC expression could be tightly regulated by doxycycline (dox) (**Figure 1a,b** and **Supplementary Figure 1**). High transgene expression was also evident given the autosuppression of endogenous MYC [18]. In the absence of dox these hESCs could differentiate to beating cardiomyocytes in EBs with similar efficiency as the parent line, making ~60% eGFP$^+$ cells by day 9 of differentiation (**Supplementary Figure 2a,b**). Activation of MYC expression by addition of dox during cardiac differentiation at day 5.5 or beyond had little impact on the expression of NKX2-5–eGFP (**Supplementary Figure 2c**), whereas dox addition at day 4.75 significantly blocked differentiation from the PDGFR-α^+ state to the NKX2-5–eGFP$^+$ state (**Figure 1c,e and Supplementary Figure 2e**). There was no such effect of dox on eGFP expression in the parent line (**Supplementary Figure 2b**). We also analyzed the expression kinetics of the posterior heart field marker podoplanin (PDPN) (**Supplementary Figure 2d**). PDPN was highly expressed in undifferentiated hESCs and was maintained in derivative NKX2-5–eGFP$^+$ cardiomyocytes, whereas in the heart myocardium PDPN expression is restricted largely to the SAN [19]. These data suggest that PDPN may have utility as a marker of both primitive CPCs and SAN-like derivatives in this system.

With the aim of further restricting CPC differentiation–inducing signaling, we added SB431542 (SB) together with dox to inhibit endogenous transforming growth factor-β (TGF-β)–activin signaling; this further restrained NKX2-5–eGFP induction as measured on day 8 (**Figure 1d,e**).

CPCs proliferate with defined mitogenic stimulation

To investigate the proliferative capacity of this largely PDGFR-α^+, pre–NKX2-5$^+$, putative CPC-encompassing population, we seeded cells at day 6 of EB differentiation at low density on a soft basement membrane. With maintained MYC expression in the continued presence of dox, cells proliferated to form small spheres (**Figure 1f**). If dox was not added or was removed on seeding, spheres did not form, and cell proliferation was not apparent on this substrate. Yet dox combined with SB was insufficient to robustly sustain the culture in a growing state beyond this first expansion, so additional mitogenic stimulants or supportive factors were sought.

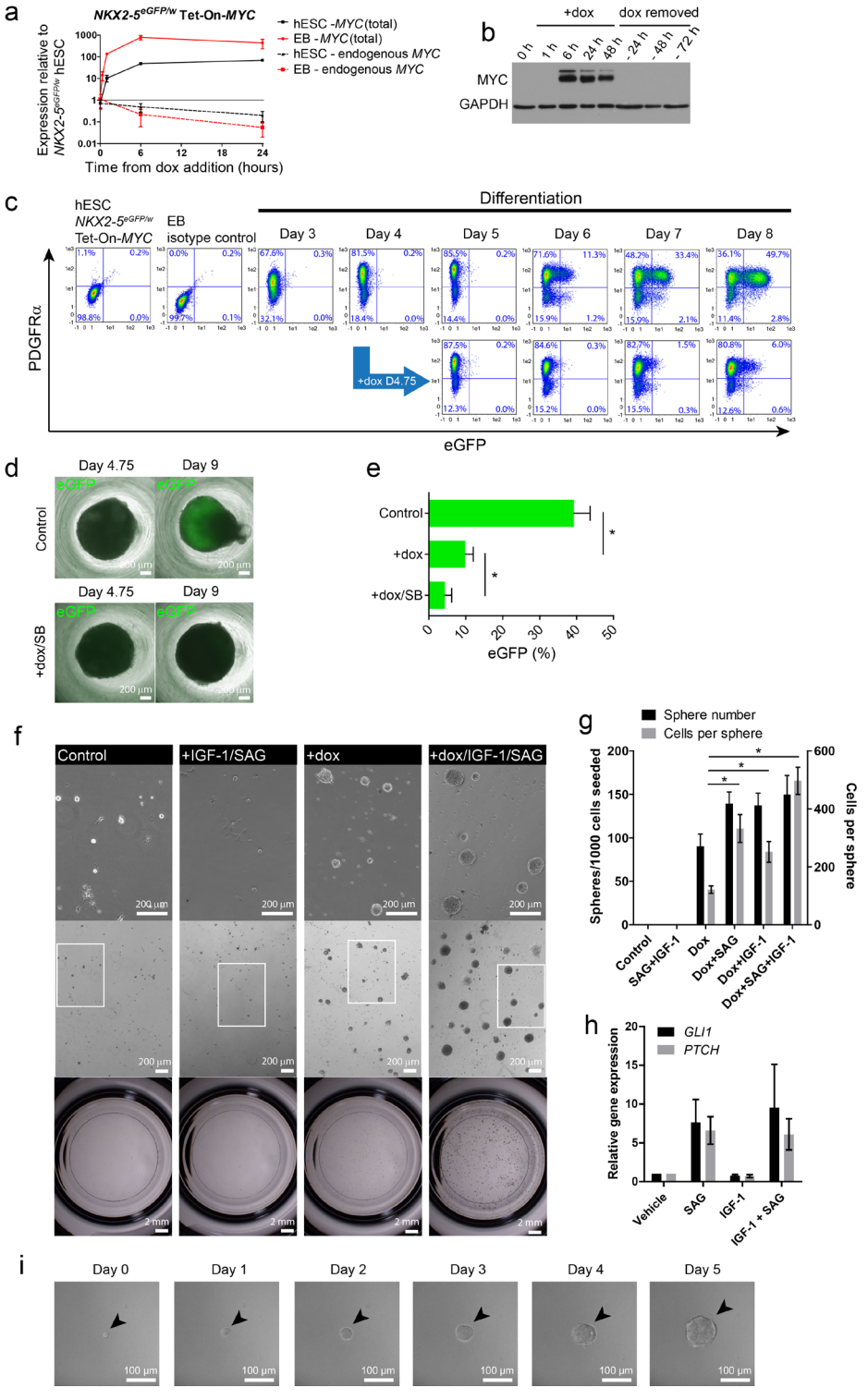
a
NKX2-5eGFP/w Tet-On-MYC
hESC -MYC(total)
EB -MYC(total)
hESC - endogenous MYC
EB - endogenous MYC
Expression relative to NKX2-5eGFP/w hESC
Time from dox addition (hours)
b
+dox
dox removed
0 h
1 h
6 h
24 h
48 h
- 24 h
- 48 h
- 72 h
MYC
GAPDH
c
hESC
NKX2-5eGFP/w
Tet-On-MYC
EB
isotype control
Differentiation
Day 3
Day 4
Day 5
Day 6
Day 7
Day 8
PDGFRα
+dox D4.75
eGFP
d
Day 4.75
Day 9
Control
+dox/SB
eGFP
200 µm
e
Control
+dox
+dox/SB
eGFP (%)
f
Control
+IGF-1/SAG
+dox
+dox/IGF-1/SAG
200 µm
2 mm
g
Sphere number
Cells per sphere
Spheres/1000 cells seeded
Cells per sphere
Control
SAG+IGF-1
Dox
Dox+SAG
Dox+IGF-1
Dox+SAG+IGF-1
h
GLI1
PTCH
Relative gene expression
Vehicle
SAG
IGF-1
IGF-1 + SAG
i
Day 0
Day 1
Day 2
Day 3
Day 4
Day 5
100 µm

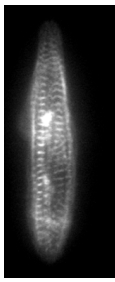

Figure 1- The expansion of early pluripotent stem cell derived cardiac cells. **A.** Time-course of MYC mRNA induction by doxycycline (dox) in NKX2-5eGFP/w Tet-On-MYC hESCs and embryoid bodies (EB). Expression is shown relative to the parent line. The lower panel shows the MYC protein induction time-course in EBs and reversal on dox removal. **B.** FACS plots for PDGFRα and **C.** Podoplanin in undifferentiated NKX2-5eGFP/w Tet-On-MYC hESCs and during a time-course of cardiac differentiation. eGFP fluorescence, reporting NKX2-5 expression, is shown on the horizontal axis. The lower panel of each shows the time-course following dox addition from day 4.75. **D.** Representative EBs imaged at day 4.75 and again at day 9 showing the effect of dox/SB addition on eGFP induction. **E.** The percentage of eGFP+ cells on day 8, with EBs maintained in the indicated conditions from day 4.75. **F.** Cultures maintained in the indicated conditions, imaged 6 days after dissociation (of day 6 EBs). The bottom panel shows the whole well. The upper images are magnifications at 4X and 10X (highlighted area). **G.** Quantification of sphere number and size (cells/sphere) after 6 days. **H.** Relative mRNA expression of hedgehog pathway response genes measured in spheres after expansion in dox/SB plus the factors indicted. **I.** Time-lapse imaging showing a single cell proliferating to form a sphere. Error bars signify SEM. *P<0.05 Paired t-test.

Roles have been proposed for IGF-1 and hedgehog signaling in CPC proliferation during cardiac development [20,21]. Dox combined with SB and IGF-1 or SAG (an agonist of Smoothened, part of the hedgehog signaling pathway) increased proliferation within spheres by 2.1-fold or 2.7-fold, respectively (**Figure 1f,g**). Whereas dox combined with SB, IGF-1 and SAG had an additive effect, increasing proliferation by 4.1-fold, MYC remained essential. The expression of SAG-induced hedgehog response genes GLI1 and PTCH1 was not modified by IGF-1, suggesting that the additive potentiation was not due to enhanced hedgehog signaling (**Figure 1h**). Time-lapse imaging showed that spheres were typically clonal (**Figure 1i** and **Supplementary Video 1**) and remained NKX2-5–eGFP^{-} under these conditions.

Concerted FGF and BMP signaling induce NKX2-5 expression

As these sphere-forming cells might be in a developmental state equivalent to pre–NKX2-5^{+} CPCs, we tested whether expression of NKX2-5–eGFP could be induced in this population by FGF and BMP signaling, as occurs during heart development [22–26]. For this experiment, spheres were generated in medium containing dox, SB, IGF-1 and SAG (DSIS) in the presence or absence of basic FGF (bFGF) and/or BMP4. SB does not interfere with BMP signaling [27]. After 6 d, bFGF had potently induced NKX2-5–eGFP expression in a concentration-dependent manner yet also reduced the number of spheres formed (**Figure 2a–d**). BMP4 alone had little impact on NKX2-5–eGFP expression but markedly potentiated induction by bFGF and, when combined with 1 ng/ml bFGF, was sufficient to induce NKX2-5–eGFP expression in >95% of cells and to a higher intensity. BMP4 in combination with bFGF also increased sphere formation compared to bFGF alone (**Figure 2c**). Inhibition of BMP signaling with dorsomophin-homolog 1 (DMH1) restricted NKX2-5–eGFP induction by bFGF and completely blocked sphere formation at higher concentrations of bFGF. A time-course experiment showed eGFP expression after 48 h of exposure to bFGF and BMP4, and this expression reverted on factor withdrawal (**Supplementary Figure 3**). Both the CPC marker PDGFR-α and the primitive CPC–SAN marker PDPN were downregulated with increasing concentrations of bFGF and BMP4, creating heterogeneity in addition to the variation in NKX2-5–eGFP levels (**Figure 2a,b**).

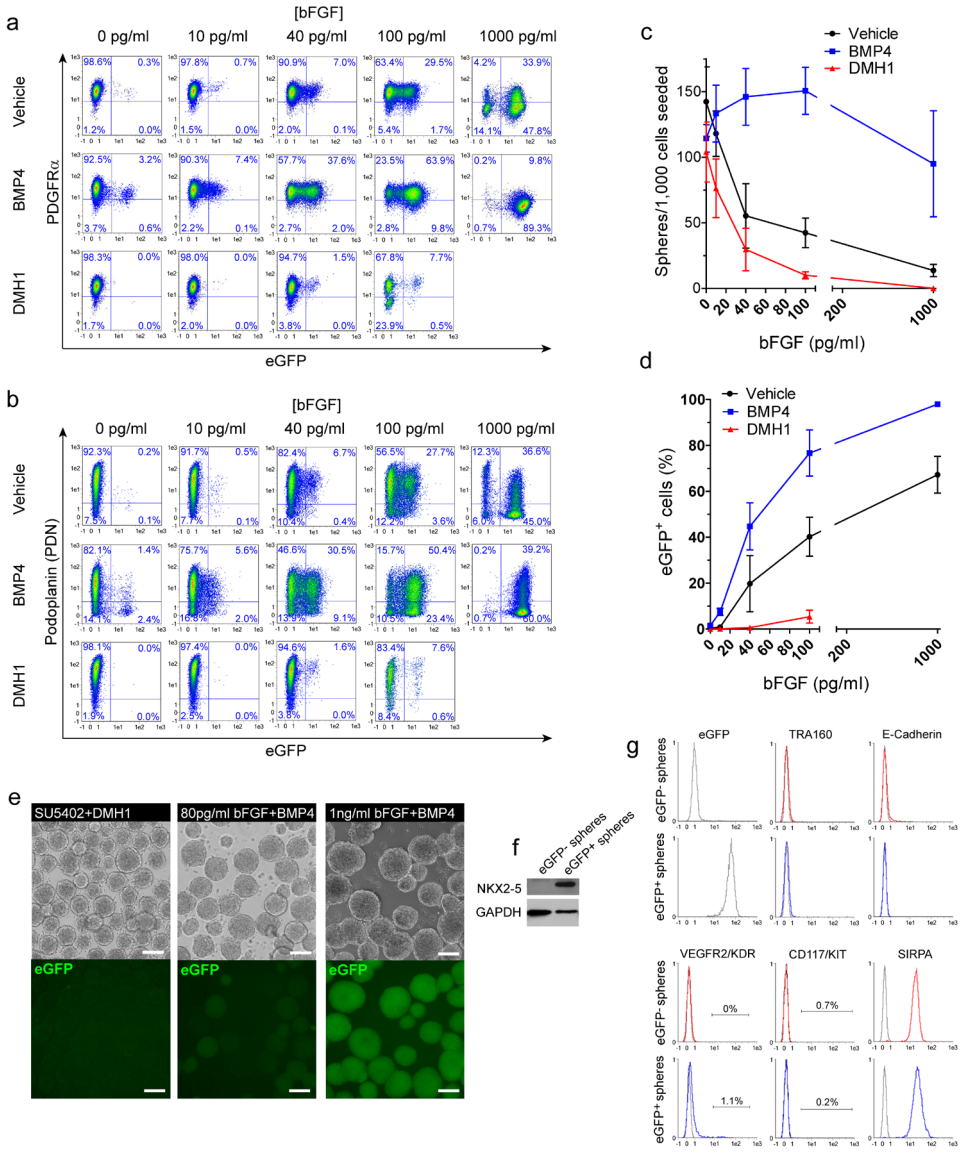

Figure 2- NKX2-5eGFP expression is activated in spheres by concerted FGF and BMP signalling. **A.** FACS measurements for PDGFRα and **B.** Podoplanin (PDN) together with eGFP, of spheres expanded in: vehicle, BMP4 or the BMP signalling-inhibitor DMH1, in concert with a range of bFGF concentrations. **C.** Sphere number in each condition. **D.** eGFP$^+$ cells in spheres of each condition. **E.** Representative spheres (in suspension after collection) following expansion in the indicated conditions. SU5402 = FGF receptor inhibitor. **F.** FACS measurement of eGFP$^-$ and eGFP$^+$ spheres for additional cell surface makers. Unlabelled/isotype control-labelled cells are shown in grey and specific antibody-labelled cells in red (eGFP$^-$) or blue (eGFP$^+$).

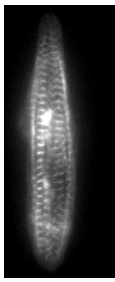

To additionally suppress endogenous FGF signaling and minimize differentiation, we pro-

duced NKX2-5-eGFP$^-$PDPN$^+$ spheres in the presence of an FGF receptor inhibitor (SU5402) as well as DMH1 (**Figure 2e**). Differences in NKX2-5 expression were confirmed by western blotting (**Figure 2f** and **Supplementary Figure 4**). **Figure 2g** shows an analysis of surface markers in NKX2-5–eGFP$^-$PDPN$^+$ cells expanded in DSIS with SU5402 and DMH1, compared to the most divergent NKX2-5–eGFP$^+$ cells expanded in DSIS with 1 ng/ml bFGF and BMP4. The pluripotent markers TRA160 and E-cadherin were absent, as were vascular endothelial growth factor receptor 2 (VEGFR2, here referred to as KDR) and stem cell factor receptor c-Kit (CD117); however, the CPC marker SIRPA was expressed in both sphere populations (data on additional surface markers are shown in **Supplementary Figure 5**). Downregulation of KDR and CD13 is consistent with their being earlier mesodermal markers [28–30], and the absence of CD117 is consistent with cardiac lineage–tracing data [31].

CPC patterning mimics features of heart field development

By regulating FGF and BMP signaling, we generated seven putative CPC sphere populations and isolated them by fluorescence-activated cell sorting (FACS) for gene expression and differentiation analysis (**Figure 3a**). Inhibition of both signaling pathways enriched the NKX2-5–eGFP$^-$PDPN^{high} (population 1), whereas exposure to BMP4 alone (with FGF signaling inhibited) or BMP4 and bFGF (80 pg/ml or 1 ng/ml) allowed isolation of cells with different NKX2-5–eGFP and PDPN expression: eGFP$^-$PDPN$^+$ (population 2), eGFP$^-$PDPN$^-$ (population 3), eGFP^{low}PDPN$^+$ (population 4), eGFP^{low}PDPN$^-$ (population 5), eGFP$^+$PDPN$^+$ (population 6) and eGFP$^+$PDPN$^-$ (population 7) (**Figure 3a,b**).

Comparison of these cells with earlier MESP1$^+$ mesodermal cells isolated from a MESP1 reporter derivative of the same hESC line28 showed much lower expression of MESP1 in all sphere populations (**Figure 3c**). NKX2-5 and PDPN expression confirmed expectations based on eGFP levels and sorting and antibody fidelity. The genes ISL1, MEF2C, SMARCD3 and TBX5, encoding cardiac transcriptional regulators, were all upregulated compared to their expression in the MESP1$^+$ cells and were expressed in the NKX2-5–eGFP$^-$PDPN^{high} population before BMP exposure. Whereas expression of the SAN-regulatory genes TBX3 and SHOX2 was lower in spheres, TBX18 was induced, most notably in the NKX2-5–eGFP$^-$PDPN$^+$ populations. Notably, HCN4, which in vivo in the mouse marks early differentiating FHF CPCs that give rise to primitive left ventricular progenitors [14,16], was induced by BMP4 exposure in this system and remained low in the NKX2-5–eGFP$^-$PDPN^{high} population. These data raise the testable hypothesis that BMP signaling, together with FGF, controls the transition from a multipotent CPC (SHF-like) to a ventricular-specified progenitor (FHF-like). Microarray analysis of five of the populations revealed a large number of genes differentially regulated by BMP4 or bFGF and BMP4, and very close clustering of the subsets positive or negative for PDPN (**Supplementary Figure 6** and **Supplementary Data Set 1**).

To induce differentiation, we removed dox to turn off MYC transgene expression and plated cells in defined endothelial- or cardiomyocyte-promoting conditions. Endothelial induction was based on vascular endothelial growth factor (VEGF) and SB (to block the TGF-β activity from the substrate) [32], with a low concentration of bFGF to preserve viability.

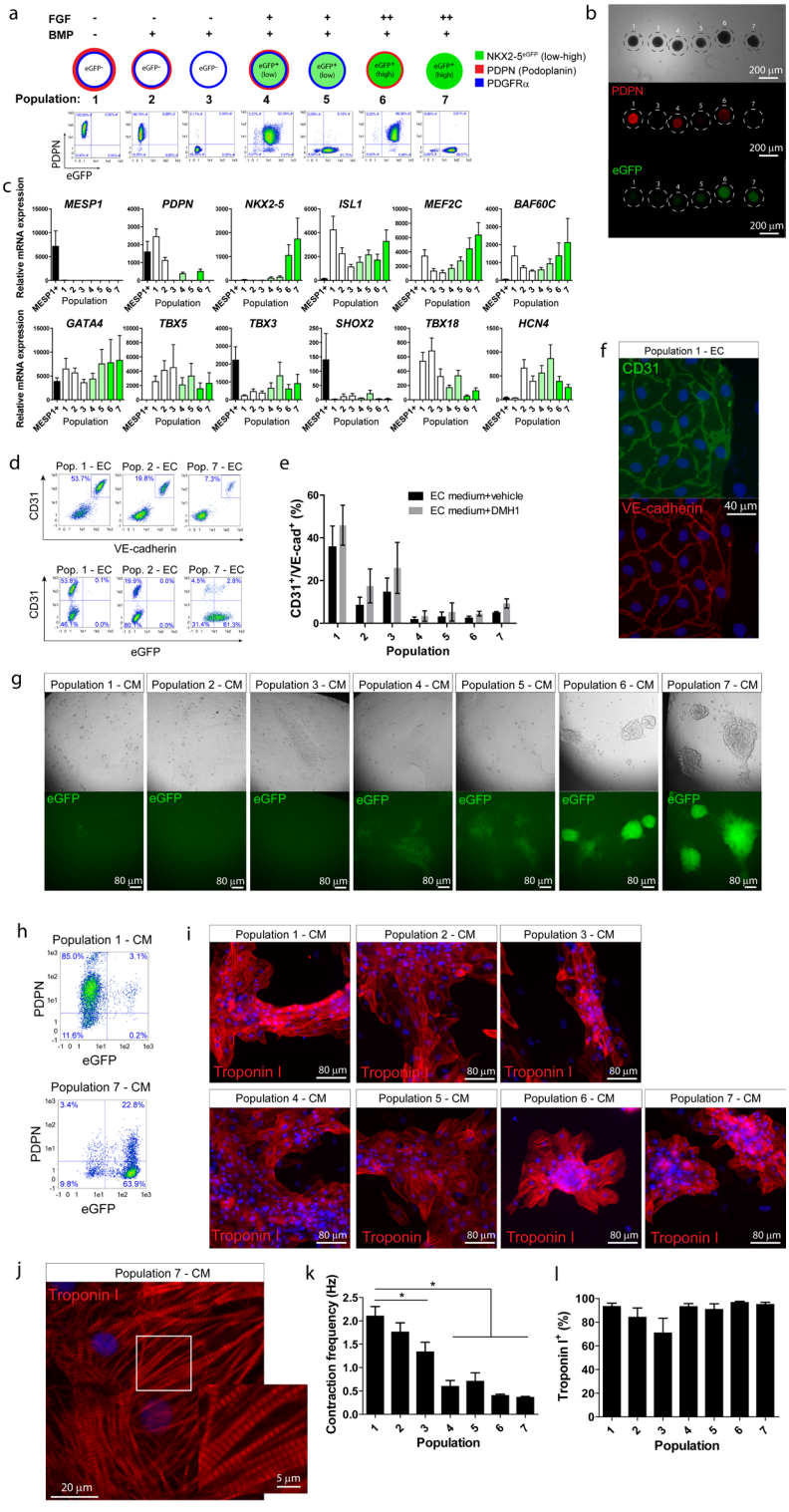
a
FGF
BMP
Population: 1 2 3 4 5 6 7
NKX2-5eGFP (low-high)
PDPN (Podoplanin)
PDGFRα
PDPN
eGFP
b
PDPN
eGFP
200 µm
c
Relative mRNA expression
MESP1
PDPN
NKX2-5
ISL1
MEF2C
BAF60C
GATA4
TBX5
TBX3
SHOX2
TBX18
HCN4
Population
d
Pop. 1 - EC
Pop. 2 - EC
Pop. 7 - EC
CD31
VE-cadherin
eGFP
e
EC medium+vehicle
EC medium+DMH1
CD31+/VE-cad+ (%)
Population
f
Population 1 - EC
CD31
VE-cadherin
40 µm
g
Population 1 - CM
Population 2 - CM
Population 3 - CM
Population 4 - CM
Population 5 - CM
Population 6 - CM
Population 7 - CM
eGFP
80 µm
h
Population 1 - CM
Population 7 - CM
PDPN
eGFP
i
Troponin I
80 µm
j
Population 7 - CM
Troponin I
20 µm
5 µm
k
Contraction frequency (Hz)
Population
l
Troponin I+ (%)
Population

Figure 3- Characterization of sphere heterogeneity and differentiation potential. **A.** Schematic showing seven sphere identities and the signalling configuration used to enrich for each. Beneath each are FACS plots showing population purity after sorting by the above markers. **B.** Individual spheres labelled live with an anti-PDN-PE antibody demonstrating the range of clonal identities. **C.** Gene expression analysis for the sorted sphere populations compared to earlier MESP1+ mesodermal progenitors (n=4). **D.** FACS measurements after differentiation of sorted populations towards endothelial cells. The upper and lower panel of each population are the same cells showing different channels. **E.** Mean percentage of endothelial cells on differentiation with or without DMH1 (n=3). **F.** Immunostaining showing typical CD31+/VE-cadherin+ endothelial cells derived from 'Population 1'. **G.** Live cell images of brightfield and eGFP after differentiation of sorted populations towards cardiomyocytes. All fields contained substantial areas of contraction. Corresponding to the areas in Supplementary video 2. **H.** FACS measurement of Population 1 and 7 for PDN and eGFP, after differentiation towards cardiomyocytes. **I.** Immunofluorescence for Troponin I after cardiomyocyte differentiation of sorted populations. **J.** Higher magnification of Population 7 to highlight the sarcomeric organization. **K.** Average contraction frequency of beating areas measured 10 days after differentiation (n=3). **L.** Mean percentage of Troponin I^+ cells (n=3). Error bars signify SEM. *P<0.05 One-way ANOVA with Bonferroni's correction.

Cardiomyocyte induction involved transient FGF and BMP signaling [33,34], with Wnt signaling inhibited [35] and exposure to TGF-β between 24 and 72 h to promote full differentiation [36]. A minimal change in bFGF concentration from the specific growth medium to the initial cardiomyocyte induction medium (i.e., in the first 24 h after dox removal) gave optimal viability and differentiation. IGF-1 and hedgehog signaling have additional roles in cardiac differentiation and so were kept active. The NKX2-5–eGFP$^-$PDPN^{high} population gave rise to VE-cadherin$^+$ (VE-cad$^+$) CD31$^+$ endothelial cells with the highest efficiency (46 ± 9%, s.e.m.), whereas eGFP$^+$ cells were much more restricted (**Figure 3d–f**). The presence of the BMP inhibitor DMH1 throughout differentiation improved endothelial differentiation efficiency in every population. In cardiomyocyte-promoting conditions, all populations differentiated with very high efficiency to spontaneously contracting cells. NKX2-5–eGFP expression status was largely maintained on differentiation, with NKX2-5–eGFP$^-$ CPCs unexpectedly giving rise primarily to NKX2-5–eGFP$^-$ cardiomyocytes (**Figure 3g–i** and **Supplementary Video 2**). The bFGF and BMP4 present in this window of differentiation as cardiomyocyte-inducing factors were apparently insufficient to induce substantial stable NKX2-5–eGFP expression in these populations. A time-course experiment during differentiation of these CPCs showed that eGFP induction was low (detected in <10% of cells) and mostly transient during this exposure period (**Supplementary Figure 7**), contrasting with the higher sensitivity of proliferating CPCs. On differentiation of populations 6 and 7, NKX2-5–eGFP expression was maintained and became stable and independent of bFGF and BMP4. Apart from derivatives of population 3, all cultures were >80% troponin I+ (**Figure 3l**). Sarcomeric organization was evident in cardiomyocytes from all populations but was particularly striking in cardiomyocytes from populations 6 and 7 (**Figure 3j** and **Supplementary Figure 8**). Contraction frequency was much higher in the cardiomyocyte monolayers from CPC population 1 (**Figure 3k**). Contractility of these cells also seemed to have more limited dynamic range, contrasting with the lower frequency and more highly dynamic contractility of the NKX2-5–eGFP$^+$ cultures.

Together with the observation of greater potential for endothelial differentiation, these data suggested that the ISL1-expressing NKX2-5– eGFP−PDPNhigh CPCs might resemble primitive SHF-like CPCs and, consequently, be competent for SAN lineage specification.

CPC differentiation to pacemaker and ventricular myocytes

To better characterize the two most divergent populations, we compared gene expression after cardiomyocyte differentiation of NKX2-5–eGFP^{-}PDPN^{high} and NKX2-5–eGFP^{+}PDPN^{-} CPCs, with standard hESC-derived cardiomyocytes from the parental line used as a reference (Supplementary Table 1). Sarcomere-related transcripts from TNNT2 and MYL7 were induced equally in both populations, consistently with a general cardiomyocyte identity (**Figure 4a**). Equal α-actinin protein expression was also observed (**Figure 4b** and **Supplementary Figure 9**). By contrast, the ventricular marker MYL2 (encoding MLC2V) was 40-fold higher in the NKX2-5–eGFP^{+}PDPN^{-} than in the NKX2-5–eGFP^{-}PDPN^{+} cardiomyocytes ($P < 0.05$), and SCN5A, encoding cardiac sodium channel, was also significantly higher in the same population ($P < 0.05$). The difference in MLC2V expression was confirmed by immunostaining (**Supplementary Figure 10**). Expression of the genes TBX5, MEF2C, GATA4, SMARCD3, HAND1, HAND2 and MYOCD, encoding cardiac transcriptional regulators, was increased similarly in each lineage and these genes were also expressed at similar levels in the reference cardiomyocytes. However, consistently with the premise that the NKX2-5–eGFP−PDPNhigh CPCs tend toward a SAN fate under these conditions, this lineage showed much higher induction of TBX3 and SHOX2 (11-fold and 289-fold, respectively) ($P < 0.05$), TBX18 (3.6-fold) and HCN4, the dominant HCN transcript underlying the hyperpolarization-activated current (If) in SAN [37] (4.3-fold). Despite these differences, which suggest regional specification, the chamber myocardial marker NPPA was induced on differentiation of both populations, and CX40 and CX43, which encode gap junction proteins, were equally expressed. Whether a functional pacemaker phenotype would develop despite seemingly inappropriate expression of such genes requires further validation.

Contracting monolayers of NKX2-5–eGFP^{+}PDPN^{-} and NKX2-5–eGFP^{-}PDPN^{+} cardiomyocytes were dissociated to single cells on micropatterned polyacrylamide gels for electrophysiological and contraction stress measurement (**Figure 4c,d**). Spontaneously active and virtually quiescent single cells were subsequently observed in both groups. After electrophysiological analysis, the quiescent cells could be subdivided into those with a depolarized (higher than −50 mV) maximal diastolic potential (MDP) (**Figure 4e**) or an MDP of approximately −75 mV (**Figure 4f**). Action potentials (APs) could be elicited by suprathreshold current pulses through the patch pipette in the latter group (**Figure 4f**) but not in those that were depolarized. Quiescent cells with an MDP of around −75 mV were observed only in the NKX2-5–eGFP^{+}PDPN^{-} group. **Figure 4g** shows typical examples of spontaneous APs of NKX2-5–eGFP^{+}PDPN^{-} and NKX2-5–eGFP−PDPN+ cells (average AP parameters are summarized in Table 1). AP parameters were notably different between the spontaneously active cells of each group. NKX2-5–eGFP^{-}PDPN^{+} cells had a higher MDP and a faster diastolic depolarization rate (DDR), which resulted in pacemaker activity with a shorter intrinsic cycle length (CL). Their maximal AP upstroke velocity (dV/dtmax) was also lower. In both cell types APs overshot the zero potential value, but the AP amplitude (APA) was lower in NKX2-5–eGFP^{-}PDPN^{+} cells. APs of NKX2-5–eGFP^{-}PDPN^{+} cells repolarized earlier and faster, resulting in shorter AP duration at 20%, 50% and 90% repolarization (APD20, APD50 and APD90, respectively). Of note, the stimulated (previously quiescent) NKX2-5–eGFP^{+}PDPN^{-} cells had a more polarized MDP and higher APA and dV/dtmax than did the

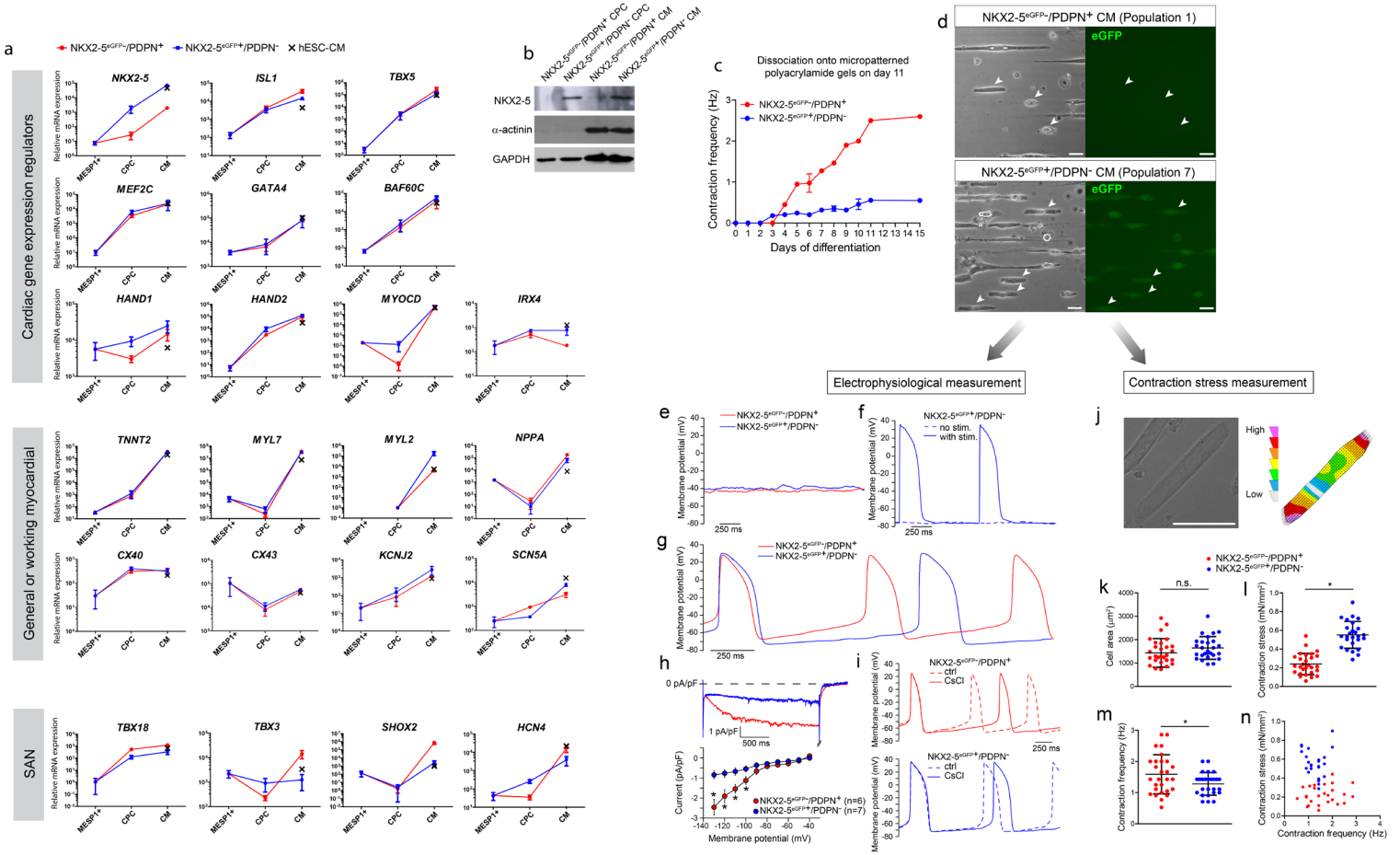
a
NKX2-5eGFP-/PDPN+
NKX2-5eGFP+/PDPN-
hESC-CM
Cardiac gene expression regulators
General or working myocardial
SAN
Relative mRNA expression
MESP1+
CPC
CM
NKX2-5
ISL1
TBX5
MEF2C
GATA4
BAF60C
HAND1
HAND2
MYOCD
IRX4
TNNT2
MYL7
MYL2
NPPA
CX40
CX43
KCNJ2
SCN5A
TBX18
TBX3
SHOX2
HCN4
b
NKX2-5eGFP-/PDPN+ CPC
NKX2-5eGFP+/PDPN- CPC
NKX2-5eGFP-/PDPN+ CM
NKX2-5eGFP+/PDPN- CM
NKX2-5
α-actinin
GAPDH
c
Dissociation onto micropatterned polyacrylamide gels on day 11
NKX2-5eGFP-/PDPN+
NKX2-5eGFP+/PDPN-
Contraction frequency (Hz)
Days of differentiation
d
NKX2-5eGFP-/PDPN+ CM (Population 1)
NKX2-5eGFP+/PDPN- CM (Population 7)
eGFP
Electrophysiological measurement
Contraction stress measurement
e
NKX2-5eGFP-/PDPN+
NKX2-5eGFP+/PDPN-
Membrane potential (mV)
250 ms
f
NKX2-5eGFP+/PDPN-
no stim.
with stim.
g
h
0 pA/pF
1 pA/pF
500 ms
Current (pA/pF)
NKX2-5eGFP-/PDPN+ (n=6)
NKX2-5eGFP+/PDPN- (n=7)
Membrane potential (mV)
i
NKX2-5eGFP-/PDPN+
ctrl
CsCl
NKX2-5eGFP+/PDPN-
j
High
Low
k
n.s.
Cell area (μm²)
l
*
Contraction stress (mN/mm²)
m
*
Contraction frequency (Hz)
n
Contraction stress (mN/mm²)
Contraction frequency (Hz)

Figure 4- "Working" ventricular-like and pacemaker-like cardiomyocyte functions recapitulated. **A.** Gene expression analysis, grouped into three gene categories, showing 3 stages of cardiac differentiation: MESP1$^+$ mesodermal progenitors, NKX2-5eGFP$^-$/PDN$^+$ or NKX2-5eGFP$^+$/PDN$^-$ CPCs, and the cardiomyocytes derived from differentiation of each CPC population. The expression of normal/control hESC-derived cardiomyocytes (hESC-CM) is shown for reference. **B.** Contraction frequency measured over time from the induction of cardiomyocyte differentiation (n=2). **C.** Brightfield and eGFP images of typical aligned cells on micropatterned soft polyacrylamide, following dissociation of high density cultures. Contracting cells are indicated with arrows. Left panel: Electrophysiological measurement. **D.** Typical recordings of quiescent cells with a depolarized (>-50 mV) MDP. **E.** Representative example of a quiescent NKX2-5eGFP+/PDN- cell with a MDP of around -75 mV without and with suprathreshold stimulation. **F.** Typical examples of spontaneously active NKX2-5eGFP$^+$/PDN$^-$ and NKX2-5eGFP$^-$/PDN$^+$ cells. **G.** Typical If recordings in response to hyperpolarizing voltage steps from -40 to -130 mV (top panel) and average current-voltage relationships of If (bottom panel). **H.** Representative examples of action potentials in the absence (ctrl) and presence (after 5 mins) of 2 mM CsCl. Right panel: Contraction stress measurement. **I.** Representative contracting cell and conversion to vector displacement values. **J.** Single cell surface area values. **K.** Single cell contraction stress values. **L.** Single cell contraction frequency values. **M.** Single cell contraction stress values plotted against frequency. Error bars signify SEM. P<0.05 Student's t-test. n.s. = not significant.

spontaneously active ones (Table 1).

If is an important characteristic of pacemaker cells, including those of humans [37]. In NKX2-5–eGFP$^-$PDPN$^+$ cells, If density was ~100% higher than in NKX2-5–eGFP$^+$PDPN$^-$ cells ($P < 0.05$) (**Figure 4h**). In 6 out of the 9 NKX2-5–eGFP$^-$PDPN$^+$ cells and in 7 out of the 15 NKX2-5–eGFP$^+$PDPN$^-$ cells measured under current clamp conditions (Table 1), we assessed the contribution of If to pacemaker activity. If block by CsCl induced a reduction of DDR, as expected, and prolongation of the CL (**Figure 4i**). The DDR was reduced by an average of 43 ± 7% and 16 ± 7% (s.e.m.), whereas the CL was prolonged by 36 ± 6% and 14 ± 7% in NKX2-5–eGFP$^-$PDPN$^+$ and NKX2-5–eGFP$^+$PDPN$^-$ cells, respectively. The more pronounced decrease in DDR and prolongation of CL in NKX2-5–eGFP$^-$PDPN$^+$ cells is probably due to the higher If and HCN4 density in these cells.

Another difference between pacemaker and working myocardial cells is in their contractile force. We measured this using traction force microscopy (**Figure 4j**). Although spontaneously active NKX2-5–eGFP$^-$PDPN$^+$ and NKX2-5–eGFP$^+$PDPN$^-$ cardiomyocytes were of similar size (**Figure 4k**), the mean contraction stress was much lower in the NKX2-5–eGFP$^-$ cardiomyocytes ($P < 0.05$) (**Figure 4l** and **Supplementary Video 3**). The lower contraction stress in the NKX2-5–eGFP$^-$ cardiomyocytes was not due to their higher beating frequency (**Figure 4m**, $P < 0.05$), as shown by the frequency-contraction stress relationships (**Figure 4n**). The absence of a positive force-frequency relationship in either population is consistent with previous measurements in PSC-derived cardiomyocytes, which display a fetal level of maturity [38].

CPCs are clonogenic and possess long-term multipotency

We next tested how frequently clonal lineages of expanded NKX2-5–eGFP$^-$PDPN$^+$ cells retain the capacity to become NKX2-5–eGFP$^+$ as well as self-renew, and whether heterogeneity in differentiation potential existed across this population. Clonal NKX2-5–eGFP$^-$PDPN$^+$ spheres were dissociated into DSIS with SU5402 and DMH1 (self-renewal condition) or DSIS with 1 ng/ml bFGF and BMP4 (NKX2-5 inducing condition). After 6 d, eGFP was

Table 1. Action potential parameters of single NKX2-5^{eGFP+}/PDN^{-} and NKX2-5^{eGFP-}/PDN^{+} cells.

	NKX2-5^{eGFP+}/PDN^{-} cells		**NKX2-5^{eGFP-}/PDN^{+} cells**
	Stimulated at 1 Hz (n=6)	Spontaneous (n=15)	Spontaneous (n=9)
MDP (mV)	–78.7±1.4†	–74.4±0.7	–68.9±1.9*
dV/dt_{max} (V/s)	44.7±10.6†	16.0±2.7	6.7±1.3*
APA (mV)	105±3†	97±2	84±4*
APD_{20} (ms)	123±16	119±16.9	79±9*
APD_{50} (ms)	179±18	178±12	124±11*
APD_{90} (ms)	207±18	217±13	172±12*
Cycle length (ms)	–	1330±155	642±108*
DDR_{100} (mV/s)	–	21.6±2.4	37.3±6.2*

Data are mean±SEM; n=number of cells, MDP=maximal diastolic potential, DDR100=diastolic depolarization rate over the 100-ms time interval starting at MDP+1 mV, dV/dtmax=maximal upstroke velocity, APA=action potential amplitude, APD20, APD50, and APD90=action potential duration at 20, 50, and 90% repolarization, respectively. † $p<0.05$ stimulated vs spontaneously active NKX2-5^{+}/PDN^{-} cells. * $p<0.05$ spontaneously active NKX2-5eGFP+/PDN- vs spontaneously active NKX2-5eGFP^{-}/PDN^{+} cells.

induced in >95% of cells from clones expanded in bFGF and BMP4 and in none of those maintained in the inhibitors, where the NKX2-5–eGFP^{-}PDPN^{+} status was largely preserved (**Supplementary Figure 11**). Endothelial differentiation capacity remained stronger in NKX2-5–eGFP^{-}PDPN^{+} spheres, whereas both populations could generate a high percentage of cardiomyocytes (median troponin I^{+}, ≥90%). Clone-to-clone variation was relatively small, indicating that the initial NKX2-5–eGFP^{-}PDPN^{+} sphere population may be uniform. The self-renewal of this early SHF-like progenitor population presents an opportunity for applying patterning with retinoic acid to direct CPC specification toward the atrial lineage. The expression profile of cardiomyocytes generated from CPCs exposed to 10 nM retinoic acid prior to differentiation suggested that this response may be present in these cells (**Supplementary Figure 12**).

To assess the long-term potential of NKX2-5–eGFP^{-}PDPN^{+} spheres and their NKX2-5–eGFP^{+} derivative spheres, we expanded the cultures over multiple passages (**Figure 5a,b**). Cells maintained in DSIS with bFGF and BMP4 had a shorter doubling time that did those in DSIS with SU5402 and DMH1 (15.3 h versus 18.6 h, respectively). In three separate experiments the lifespan of NKX2-5–eGFP^{-}PDPN^{+} spheres in DSIS with SU5402 and DMH1 was ~50 population doublings, at which point the cells abruptly stopped growing, whereas cells in DSIS with bFGF and BMP4 grew for >80 doublings without reaching senescence. NKX2-5–eGFP induction capacity was well preserved in NKX2-5–eGFP^{-}PDPN^{+} CPCs maintained with SU5402 and DMH1, with ~80% of cells, on average, capable of full induction beyond 40 doublings (**Figure 5c,d**). These cells could also generate >30% endothelial cells beyond 35 doublings, whereas CPCs induced to NKX2-5–eGFP^{+} status were progressively restricted (**Figure 5e**), as observed above (**Figure 3e**). Cardiomyocyte differentiation was >80% efficient up to around 30 doublings in all three populations (**Figure 5f**), beyond which distinctly striated α-SMA^{+} smooth muscle–like cells (troponin I^{-}) became increasingly prevalent, resulting in more mixed populations (**Figure 5g**). NKX2-5–eGFP expression was difficult to maintain uniformly beyond 50 doublings (**Supplementary Figure 13**).

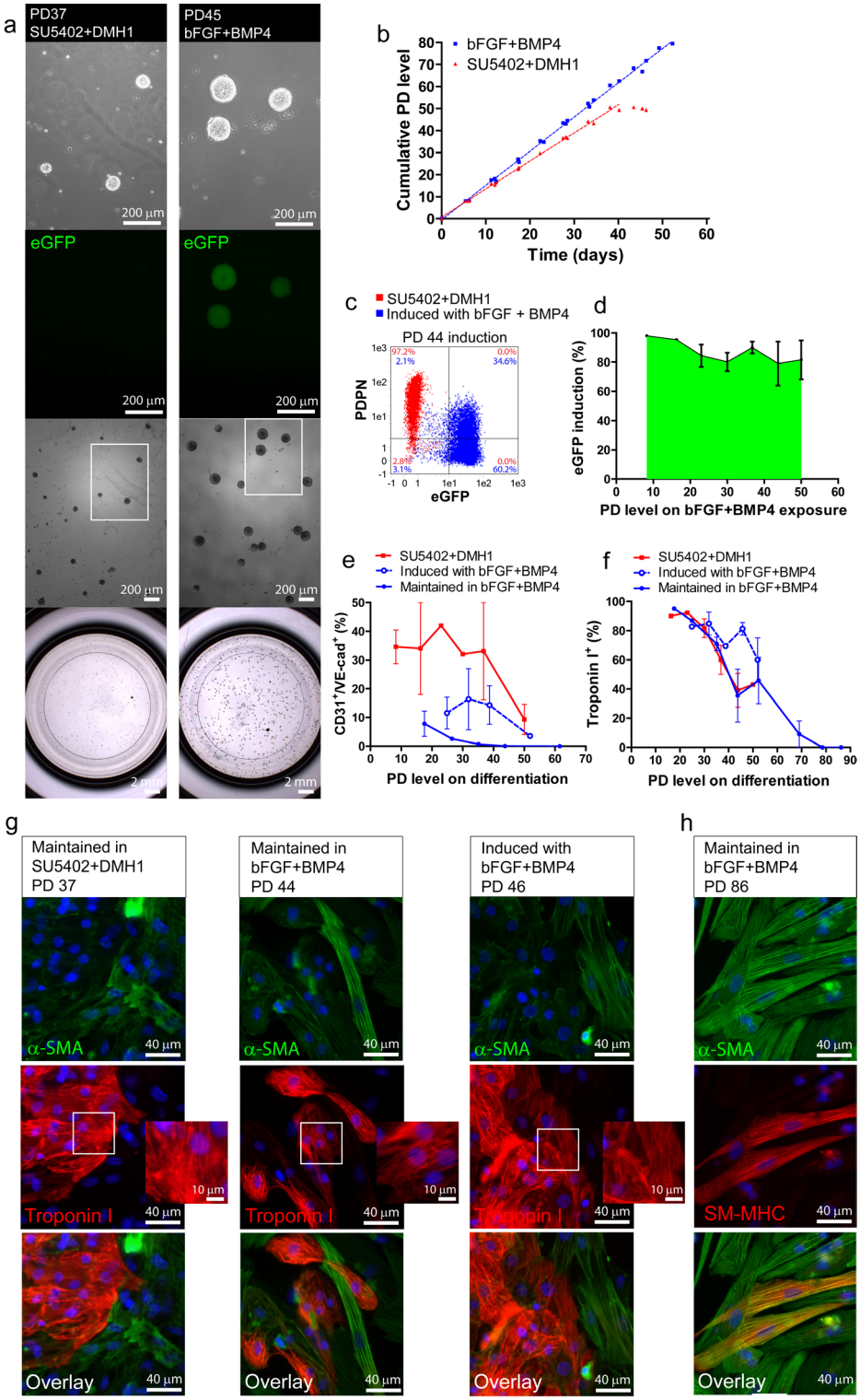
a
PD37
SU5402+DMH1
PD45
bFGF+BMP4
200 µm
eGFP
2 mm
b
bFGF+BMP4
SU5402+DMH1
Cumulative PD level
Time (days)
c
SU5402+DMH1
Induced with bFGF + BMP4
PD 44 induction
PDPN
eGFP
97.2%
2.1%
0.0%
34.6%
2.8%
3.1%
0.0%
60.2%
d
eGFP induction (%)
PD level on bFGF+BMP4 exposure
e
SU5402+DMH1
Induced with bFGF+BMP4
Maintained in bFGF+BMP4
CD31+/VE-cad+ (%)
PD level on differentiation
f
SU5402+DMH1
Induced with bFGF+BMP4
Maintained in bFGF+BMP4
Troponin I+ (%)
PD level on differentiation
g
Maintained in SU5402+DMH1 PD 37
Maintained in bFGF+BMP4 PD 44
Induced with bFGF+BMP4 PD 46
h
Maintained in bFGF+BMP4 PD 86
α-SMA
Troponin I
SM-MHC
Overlay
40 µm
10 µm

Figure 5- Clonal analysis of NKX2-5eGFP^{-}/PDN^{+} spheres shows self-renewal and universal potential for endothelial and cardiomyocyte differentiation. **A.** Individual clonal NKX2-5eGFP^{-}/PDN^{+} spheres were isolated and dissociated for expansion in **B.** (**i**) DSIS+SU5402+DMH1 or (**ii**) DSIS+1 ng/ml bFGF+BMP4. Representative images are shown after expansion of one clone. **C.** (**i**) eGFP and Podoplanin (PDN) measurement in each clone after expansion in (**i**) DSIS+SU5402+DMH1 or (**ii**) DSIS+bFGF+BMP4. FACS plots are shown for 3 clones. **D.** Representative brightfield images taken 4 days after the start of endothelial or cardiomyocyte differentiation for clone 27, after expansion in (**i**) DSIS+SU5402+DMH1 or (**ii**) DSIS+bFGF+BMP4. The cell clustering seen in the cardiomyocyte-promoting condition is strongly associated with a cardiomyocyte fate. **E.** Percentage of CD31+ endothelial cells derived from each clone expanded in (**i**) DSIS+SU5402+DMH1 or (**ii**) DSIS+bFGF+BMP4. FACS plots are shown for 3 clones. **F.** Percentage of Troponin I+ cells from each clone after expansion in (**i**) DSIS+SU5402+DMH1 or (**ii**) DSIS+bFGF+BMP4. Immunofluorescence images of two clones are shown, and were representative.

Spheres induced over one passage with bFGF and BMP4 gave the highest percentage of cardiomyocytes at higher doubling levels. Beyond 78 doublings, only smooth-muscle cells were generated. The more definitive smooth-muscle marker SM-MHC was also evident in many of these cells (**Figure 5h**).

Discussion

Studies in developmental biology have provided the foundation for the understanding and control of hPSC differentiation. This has led to effective methods for generating cardiac cell types, but difficulties in maintaining CPCs have hindered specific reconstruction of some aspects of heart development [5]. In this study we developed a system enabling the isolation and robust expansion of pure populations of hPSC-derived CPCs. A central feature of our method is the use of controlled MYC expression to facilitate the maintenance of CPCs. When expressed in a defined time window, MYC arrested CPCs at a pre–NKX2-5^{+} multipotent stage and acted as an essential permissive element in their continued expansion through IGF-1 and hedgehog signaling. In mouse development, c-Myc mRNA is clearly detectable in the embryonic heart and decreases markedly in the neonate [39].

Cardiogenesis is regulated by the tight spatial and temporal control of secreted factors at specific concentrations [40]. Although the early cardiogenic roles of cytokines including BMP, activin and Wnt have been well characterized in the PSC system [17,35,41], control of CPC specification has not be as well studied. The expression of FGF and BMP, particularly by endoderm and ectoderm adjacent to the heart-forming region, is thought to underlie early NKX2-5 expression [22,24–26]. These tissues may have similar inducing roles on the later-differentiating SHF progenitor population, with additional signaling sources being the SHF progenitors themselves and the primary myocardium [7,42]. Here we show that the developmental roles of FGF and BMP are reenacted in hPSC CPCs, and by modulating these signaling pathways we were able to recreate the gene expression signatures of early heart field development (**Figure 6**) and direct the patterned CPCs toward NKX2-5–eGFP^{-} PDPN^{+} pacemaker-like myocytes or NKX2-5–eGFP^{+} ventricular-like working myocytes with appropriate electrophysiological and contractile characteristics. CPC-derived NKX2-5–eGFP^{+} cardiomyocytes had well-organized sarcomeres and encompassed a population of highly polarized quiescent cells excitable by stimulation—the signature of mature working myocytes. By contrast, the pacemaker-like cells exhibited rapid spontaneous activity owing to their higher If. Additionally, we found that NKX2-5–eGFP^{-}PDPN^{+} CPCs were uniquely

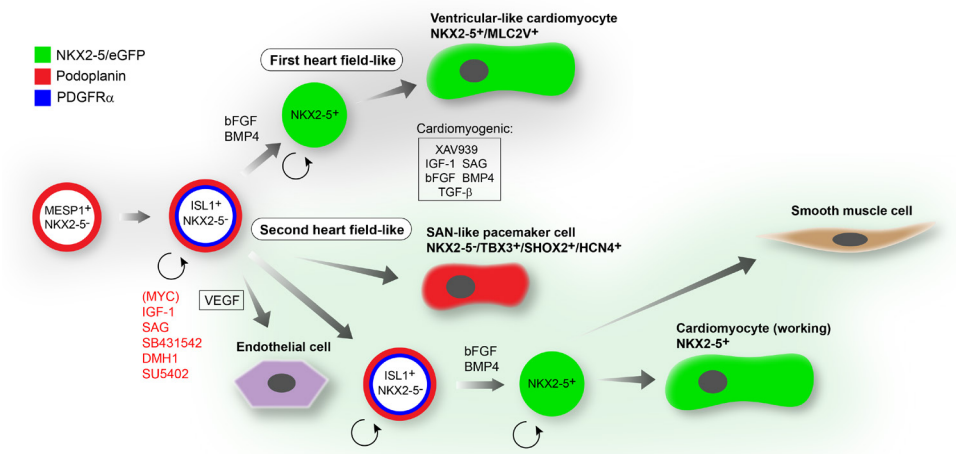

Figure 6- Long term expansion and differentiation analysis of CPCs. **A.** CPC spheres expanded for 37 population doublings (PD) in DSIS+SU5402+DMH1 (eGFP-) or 45 PD in 1 ng/ml bFGF+BMP4 (eGFP+). Images for each condition are of one dish at different magnifications. **B.** Growth curves for each culture condition (n=3 expansions). **C.** NKX2-5eGFP induction capacity from DSIS+SU5402+DMH1 on exposure to bFGF+BMP4, measured at progressive population doubling levels. **D.** CPCs expanded to PD 44 in DSIS+SU5402+DMH1 (red), tested for NKX2-5eGFP-induction capacity by bFGF+BMP4 exposure (blue). Podoplanin (PDN) is measured on the vertical axis. Each quadrant shows the frequency of each population coded by colour. **E.** Percentage of CD31+/VE-cadherin+ endothelial cells, or **F.** Troponin I+ cardiomyocytes, generated from each three culture conditions at progressive population doubling levels. **G.** Immunofluorescence of α-smooth muscle actin (α-SMA) and Troponin I after cardiomyocyte differentiation of spheres at the indicated doubling level in the condition shown. Note: eGFP fluorescence (in the bFGF+BMP4 conditions) is weak after fixation and does not interfere with interpretation of filament labelling by the α-SMA antibody. **H.** Immunofluorescence images of α-SMA and smooth muscle myosin heavy chain (SM-MHC) after differentiation of spheres at PD 86.

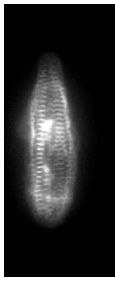

susceptible to differentiation to an endothelial fate despite having undetectable levels of KDR expression, which is therefore not essential for this capability. This competence might shed light on the origin of the endocardium [43]. The generation of atrial cardiomyocytes was not the focus of this study, but we showed that retinoic acid may have a role in directing this lineage commitment when applied initially to the self-renewing SHF-like NKX2-5–eGFP^{-}PDPN^{+} CPCs, consistently with earlier reports [44,45].

CPCs could be expanded to >40 population doublings while retaining multipotent differentiation capacity, a substantial extension compared with previous reports [11,12,29,30,46–51]. Although the use of a MYC transgene limits the translational applicability of our approach, the growth stability achieved creates an opportunity to identify factors enabling the expansion of either pre–NKX2-5^{+} or NKX2-5^{+} CPCs in the absence of exogenous MYC (i.e., dox-independent growth) or genes that restrain self-renewal, such as those governing cell-cycle arrest mechanisms. This tractable system could be used to help identify the genes conferring CPC potential, and hence the nature of the apparent 'clock' we have observed, which we define as the progressive time-dependent shift in differentiation affinity toward smooth muscle, perhaps in relation to the development of smooth muscle in the heart [52].

We replicated the essential elements of these results in induced hPSCs (Supplementary

Figure 14 and Supplementary Video 4). Such applications could benefit studies aiming to model cardiac disease, for example, by isolating and cryopreserving CPCs, which are later differentiated to the necessary target population. Realizing the potential shown here means that an expansion of more than 107-fold from the starting CPC population is feasible. In summary, the identification of MYC as a permissive factor in CPC self-renewal should enable the use of expandable PSC-derived CPCs for a variety of applications relating to modeling or regenerating the human heart.

Methods

Tet-On-MYC hPSC line generation and maintenance

NKX2-5eGFP/w hESCs generated previously [37], or hiPSCs generated previously (LQT-hiPSCsN9961 and LQT2-hiPSCsCORR) [41], were maintained on mouse embryonic fibroblasts in DMEM/F12-based medium containing 20% Knockout Serum Replacement (Invitrogen) and 10 ng/ml bFGF (Miltenyi Biotech). hPSCs were passaged using TrypLE Select (Invitorgen). A Tet-On-MYC system was introduced into each line by transducing the hPSCs with two lentiviruses, one carrying a MYC T58A transgene under the control of a TRE-CMV promoter (Addgene plasmid #19775), and the second carrying the tetracycline transactivator (Addgene plasmid #19780) [42]. Titres giving transduction efficiencies of approximately 40% (based on a GFP expressing control lentivirus) were used to avoid multiple viral insertions. Clones were isolated following single cell FACS deposition and selected for their ability to efficiently upregulate MYC on exposure to doxycycline.

hPSC differentiation

Differentiations were performed in serum-free "BPEL" medium using an embryoid body (EB) system as previously described [43]. The following growth factors were present for the first 3 days of differentiation: 30 ng/ml BMP4 (R&D), 25 ng/ml Activin A (Miltenyi Biotech), 30 ng/ml VEGF (Miltenyi Biotech), 40 ng/ml SCF (Miltenyi Biotech) and 1.5 μM CHIR99021 (Axon Medchem). On day 4.75 control wells were refreshed again with plain medium ± vehicle, or for MYC induction with medium containing 1 μg/ml doxycycline (Sigma Aldrich) ± 5 μM SB431542 (Tocris Bioscience). EBs were either maintained in these conditions for subsequent FACS, RNA or protein analysis, or dissociated on day 6 for progenitor expansion.

CPC culture maintenance and differentiation

CPCs were seeded on a thin layer (14 μl/cm2) of undiluted Matrigel (BD Bioscience) in organ culture dishes (BD Falcon) in BPEL medium containing 5 μM SB431542 with or without experimental factors: 1 μg/ml doxycycline, 100 ng/ml LONG R3 IGF-1 (hereafter, IGF-1), 1 μM SAG (Millipore), 0.5 μM DMH1 44, 5 μM SU5402, bFGF (Miltenyi Biotech), BMP4 (R&D). Reagents were obtained from Sigma-Aldrich unless stated otherwise. Cultures were refreshed every 2 days. Growing cell spheres were manually collected after 6 days under a dissecting microscope, dissociated using TrypLE Select and either plated for differentiation or replated on fresh Matrigel at a density of 350-1700 cells/cm^2 depending on the condition. Long term expansions were carried out at 3% O2 to minimise cellular senescence. For clonal

analysis, single cell deposition of eGFP$^-$/PDN$^+$ cells into 96-well plates was performed by FACS, from EBs at day 6 of differentiation. Clonal spheres were then picked after 6 days for propagation.

Cardiomyocyte differentiation was induced by plating cells at a density of 105 cells/cm^2 on either Matrigel-coated (1:100 dilution) 96-well plates (BD Falcon) in BPEL medium supplemented with 100 ng/ml IGF-1, 1 μM SAG, 1 μM XAV 939 (Tocris Bioscience), 100 or 1000 pg/ml bFGF (for NKX2-5GFP$^-$ and NKX2-5GFP$^+$ CPCs respectively) and 20ng/ml BMP4. From 24-72 h of differentiation cells were all in the same medium above containing 100 pg/ml bFGF plus the addition of 2.5 ng/ml TGFβ1 (Peprotech). At 72 h the medium was changed to 100 ng/ml IGF-1, 1 μM XAV 939 and 10 pg/ml bFGF. At 96 h onwards the beating cardiomyocytes were maintained in contractility-promoting medium (MJB unpublished data) containing 100 ng/ml IGF-1, 30 μM 3,3',5-Triiodo-L-thyronine sodium salt (T3) and 1 μM dexamethasone (all Sigma Aldrich).

Endothelial differentiation was induced by plating cells at a density of 0.6x105 cells/cm^2 on Matrigel-coated 96-well plates (BD Falcon) in BPEL medium supplemented with 100 ng/ml IGF-1, 50 ng/ml VEGF, 50 pg/ml bFGF, 5 μM SB431542 and 0.5 μM DMH1. Medium was refreshed at 48 h. At 96 h DMH1 was removed. Cells were analysed by FACS or fixed after a further 2 days.

Flow cytometry and cell sorting

Staining was performed in PBS containing 1 mM EDTA and 0.5% BSA. The antibodies and dilutions used were as follows: anti-PDGFRα-BV421 (BD Bioscience cat no. 562799; 1:50), anti-Podoplanin-PE (eBioscience cat no. 12-9381-41; 1:500), anti-VEGFR2-PE (R&D cat no. FAB357P; 1:50), anti-VEGFR3-PE (R&D cat no. FAB3492P; 1:50), , anti-VE-cadherin-PE (eBioscience cat no.12-1449-80; 1:150), anti-CD31-APC (eBioscience cat no. 17-0319-42; 1:150), anti-CD90-PE (BD cat no. 555596; 1:500), anti-CD146-PE (BD cat no. 550315; 1:20), anti-NG2-PE (R&D cat no. FAB2585P; 1:20), anti-PDGFRβ-PE (BD cat no. 558821; 1:20), anti-E-cadherin-APC (R&D cat no. FAB18381A; 1:40), anti-TRA-1-60-PE (Miltenyi Biotec cat no. 130-100-347; 1:100), anti-CD73-PE (BD cat no. 550257; 1:20), anti-CD105-PE (Life Technologies cat no. MHCD10504; 1:20), anti-CD13-BV421 (Biolegend cat no. 301716; 1:50), anti-CKIT-APC (BD Bioscience cat no. 550412; 1:100), anti-SIRPα (Biolegend cat no. 323801; 1:500), anti-mouse IgG PE (Jackson Immuno Research cat no: 115-116-146; 1:200), mouse IgG1 (BD Bioscience cat no. 556650), mouse IgG2a-BV421 (BD Bioscience), mouse IgG1-PE isotype control (Miltenyi Biotec 130-098-845), mouse IgG2b-APC isotype control (R&D cat no. IC0041A). Samples were measured with a MACSQuant VYB (Miltenyi Biotech) equipped with a violet (405nm), blue (488nm) and yellow (561nm) laser.

Immunostaining and microscopy

Cells were fixed with 2% paraformaldehyde and permeabilised with 0.1% Triton X. Blocking was achieved with 4% normal goat serum. Primary antibody incubations were overnight in 4% normal goat serum at 4°C using the following antibodies: anti-troponin I (clone H170, Santa Cruz; 1:500) together with α-smooth muscle actin (Sigma A2547; 1:300), or

VE-cadherin (Cell Signalling; 1:200) together with CD31 (DAKO M0823; 1:20). Secondary antibodies were: Alexa 488 anti-mouse and Alexa 555 anti-rabbit (Invitrogen). GFP fluorescence was reduced to background levels after fixation and could be differentiated from the specific smooth muscle type-α-smooth muscle actin staining.

Quantitative real time PCR

RNA was isolated using a Minelute RNA extraction kit (Qiagen) and cDNA synthesized using an iScript cDNA synthesis kit (BioRad). Real time PCR was performed on a BioRad CFX96 machine using IQ SYBR Green (BioRad). Gene expression values were normalized to the mean expression of the housekeeping genes human acidic ribosomal phosphoprotein (hARP), glucuronidase (GUS), and RNF7. RNA from MESP1-expressing sorted cells was obtained from a derivative knock-in reporter line and used as a reference [23]. The hESC-cardiomyocyte control RNA was obtained from eGFP+ sorted cells from a standard monolayer differentiation of the NKX2-5$^{eGFP/w}$ hESC line .

Primer sequences were as follows:

Gene	Forward primer	Reverse primer
hARP	CACCATTGAAATCCTGAGTGATGT	TGACCAGCCCAAAGGAGAAG
GUS	CCACCTAGAATCTGCTGGCTAC	GTGCCCGTAGTCGTGATACCAA
MYC (endogenous only)	AGAAATGTCCTGAGCAATCACC	AAGGTTGTGAGGTTGCATTTGA
MYC (total)	ACGCACCGAATAGTTACGG	CCAGGTCCACGGGCAGA
MESP1	CTCTGTTGGAGACCTGGATG	CCTGCTTGCCTCAAAGTG
PDPN	AGTGTCATCTTCTGGCTGGC	AGCAACAACTCAACGGGAAC
NKX2-5	TCTATCCACGTGCCTACAGC	GTTGTCCGCCTCTGTCTTCT
ISL1	TGATGAAGCAACTCCAGCAG	GGACTGGCTACCATGCTGTT
MEF2C	CCACTGGCTCACCCTTCTCTGC	ACCCGTTCCCTGCACTAGTG
BAF60C	GCGCGCAAAGCCACGAAA	ATCCGGGCTCCAGACGGCATC
GATA4	GACAATCTGGTTAGGGGAAGC	GAGAGATGCAGTGTGCTCGT
TBX5	TACCACCACACCCATCAAC	ACACCAAGACAGGGACAGAC
FGF8	TACATCTGCATGAACAAGAAGGG	TTCTCCAGCACAATCTCCGT
HAND1	TGAACTCAAGAAGGCGGATG	AATCCTCTTCTCGACTGGGC
HAND2	ACATCGCCTACCTCATGGAC	TGGTTTTCTTGTCGTTGCTG
TBX3	AAAGGAGAATGGGACCTCTG	CGCTGGGACATAAATCTTTGAG
TBX18	TTGCTAAAGGCTTCCGAGAC	AGGTGGAGGAACTTGCATTG
SHOX2	AATCAAGCAGAGGCGAAGTC	TCTCGTCAAAAAGCCTCTCC
MYOCD	CAACACCGATTCAGCTACCT	TTCAGAGACCTTCAGATCCAG
MYL2/MLC2V	TACGTTCGGGAAATGCTGAC	TTCTCCGTGGGTGATGATG
MYL7/MLC2A	CTTGTAGTCGATGTTCCCCG	TCAAGCAGCTTCTCCTGACC
TNNT2	TTCGACCTGCAGGAGAAGTT	GCGGGTCTTGGAGACTTTCT
ACTN2	CTGCTGCTTTGGTGTCAGAG	TTCCTATGGGGTCATCCTTG
MYBPC3	GGCATGCTAAAGAGGCTCAA	TCTTGTGGCCTTTGCTCAC

Western blot

Samples were lysed with ice cold ELB (50mM HEPES pH 7.0; 250mM NaCl; 5mM EDTA; 0.1% NP-40) or RIPA (25mM Tris-HCl pH 7.6; 150mM NaCl; 1% Triton X100; 0.1% SDS; 1% Sodium Deoxycholate) with 1:100 Protease Inhibitor Cocktail (Sigma-Aldrich) for 30 mins on ice. The samples were centrifuged at 7000g for 10 mins and the supernatant was quantified for protein content (Bradford dye-binding method). 30μg of each sample was

run in a 10% polyacrylamide gel together with the protein ladder (Precision Plus Protein dual colour – Bio-Rad). The protein was transferred to an Amersham Hybond membrane (GE Heathcare- Life Sciences) overnight. The membrane was blocked with blocking buffer (2% milk in PBS) and probed with a Rabbit IgG anti-cMYC 1:1000 (Cell Signaling 5605S) detected with a Goat anti-Rabbit IgG – HRP (Cell Signaling 7074s).

Patterned Polyacrylamide gel fabrication

Patterned polyacrylamide gels were prepared as previously described [45]. Briefly, a 1% gelatin solution was activated with 3.5mg/mL Sodium Periodate (both Sigma-Aldrich). A polydimethylsiloxane (PDMS) stamp was casted from a SU8 master produced by standard soft lithography techniques and incubated with the activated 1% gelatin solution for 45 mins. The excess of gelatin was removed with a nitrogen gun and the stamp was used to μcontact-print a pattern of 20μm thick with 20μm spacing gelatin lines onto 10mm (electrophysiology) or 15mm (contraction assay) coverslips. The polyacrylamide solution was prepared with a final concentration of 0.1% bis-acrylamide (Bio-Rad), 5% acrylamide (Bio-Rad) and 10mM HEPES pH 8.5 in distilled water, followed by centrifugation for 1 min at 10.000RPM for degassing. 0.006% (m/v) of ammonium persulfate (Sigma-Aldrich) and a 1:1000 dilution of 0.2-μm fluorescent beads (Ex/Em: 660/680nm - Molecular Probes) were added to the solution (for the contraction assay) and briefly vortexed. The gel polymerization was initiated with TEMED (Bio-Rad) and 4.08μl/9.2μl of the final solution was added to a 15mm/25mm coverslip treated with plus Bind-Silane solution (GE Healthcare). The μcontact-printed coverslip was applied on top of the drop with the gelatin lines facing the gel. After 20mins of polymerization the 10mm/15mm coverslip was removed. Each 25mm coverslip was mounted onto a well of a glassbottom 6-well plate (Mattek), replacing the initial glass. The 15mm coverslips were used directly. Plates were UV-sterilized and re-hydrated with culture medium for 30 mins before use. The polymerized gel has a Young's modulus of 5.8 kPa [46].

Contraction force measurements

The contraction force measurements were performed as previously described [47]. Briefly, using a Leica AF-6000LX microscope with controlled temperature and CO2, 40x image series of brightfield and fluorescent beads were taken at 20 frames per second of aligned single self-pacing cardiomyocytes. Single frames from maximal relaxation and contraction of the brightfield and fluorescent beads image series were analyzed by the LIBTRC software package (kindly provided by Dr. Micah Dembo), creating a mask of the cell outline from the brightfield image and a vector map from the difference between the relaxed and contracted fluorescent beads images. The vector map and the cell mask were used to calculate the total force that the cell applies on the substrate at its maximum peak of contraction. The contraction stress generated by the cardiomyocyte during contraction was calculated by dividing the total force by the cell surface area.

Cellular electrophysiology

Recording procedures. Action potentials and the hyperpolarization-activated current, If,

were recorded in single cells by the amphotericin-perforated patch-clamp technique using an Axopatch 200B amplifier (Molecular Devices, USA) 5-7 days after dissociation on day 11 of differentiation. Coverslips containing the cells were put in a recording chamber on the stage of an inverted microscope and superfused with Tyrode's solution (36±0.2°C) containing (in mM): NaCl 140, KCl 5.4, CaCl2 1.8, MgCl2 1.0, glucose 5.5, and HEPES 5.0; pH 7.4 (NaOH). Patch pipettes (borosilicate glass, 2-3 MΩ) were filled with solution containing (in mM): K-gluc 120, KCl 20, NaCl 5, amphotericin-B 0.44, HEPES 10, pH 7.2 (KOH). Series resistance was compensated by ≥80%, and potentials were corrected for the calculated liquid junction potential. Action potentials were low-pass filtered (cut-off frequency: 2 kHz) and digitized at 10 kHz, while If was filtered and digitized at 1 kHz and 4 kHz, respectively. Voltage control, data acquisition and analysis were accomplished using custom software. Cell membrane capacitance (Cm) was estimated by dividing the time constant of the decay of the capacitive transient in response to 5 mV hyperpolarizing voltage clamp steps from -40 mV by the series resistance.

Action potentials measurements. In both cell groups we observed spontaneously active as well as virtually quiescent single cells. We recorded spontaneous action potentials or action potentials were elicited at 1 Hz by 3-ms, ≈1.2Ω threshold current pulses through the patch pipette. Action potentials were characterized by duration at 20, 50, and 90% repolarization (APD20, APD50, and APD90, respectively), maximum diastolic potential (MDP), action potential amplitude (APA), maximum upstroke velocity (dV/dtmax), and, in case of spontaneously active cells, cycle length (CL) and diastolic depolarization rate measured over the 100-ms time interval starting at MDP+1 mV (DDR100). Parameter values obtained from 10 consecutive action potentials were averaged.

If measurements. If was activated upon 2-s hyperpolarizing pulses from a holding potential of –40 mV. If amplitude was calculated as the difference between the current at the beginning and end of the voltage step. Current densities were calculated by dividing current amplitudes by Cm.

Statistical analyses

Data are mean±SEM. Groups of HF SAN cells were compared with groups of CTRL SAN cells using Fisher's exact test, Two-Way Repeated Measures ANOVA followed by pairwise comparison using the Student-Newman-Keuls test, and unpaired t-test. Paired t-tests were used to compare drug effects within a group. An F-test was used to compare frequency dependency between groups. $P<0.05$ is considered statistically significant

References

[1] Drawnel, F.M. et al. Disease modeling and phenotypic drug screening for diabetic cardiomyopathy using human induced pluripotent stem cells. Cell Reports 9, 810–820 (2014).

[2] Matsa, E., Burridge, P.W. & Wu, J.C. Human stem cells for modeling heart disease and for drug discovery. Sci. Transl. Med. 6, 239ps6 (2014).

[3] Lundy, S.D., Gantz, J.A., Pagan, C.M., Filice, D. & Laflamme, M.A. Pluripotent stem cell derived cardiomyocytes for cardiac repair. Curr. Treat. Options Cardiovasc. Med. 16, 319 (2014).

[4] Bhave, M., Akhter, N. & Rosen, S.T. Cardiovascular toxicity of biologic agents for cancer therapy. Oncology 28, 482–490 (2014).

[5] Birket, M.J. & Mummery, C.L. Pluripotent stem cell derived cardiovascular progenitors—a developmental perspective. Dev. Biol. 400, 169–179 (2015).

[6] Vincent, S.D. & Buckingham, M.E. How to make a heart: the origin and regulation of cardiac progenitor cells. Curr. Top. Dev. Biol. 90, 1–41 (2010).

[7] Cai, C.-L. et al. Isl1 identifies a cardiac progenitor population that proliferates prior to differentiation and contributes a majority of cells to the heart. Dev. Cell 5, 877–889 (2003).

[8] Lints, T.J., Parsons, L.M., Hartley, L., Lyons, I. & Harvey, R.P. Nkx-2.5: a novel murine homeobox gene expressed in early heart progenitor cells and their myogenic descendants. Development 119, 419–431 (1993).

[9] Ma, Q., Zhou, B. & Pu, W.T. Reassessment of Isl1 and Nkx2–5 cardiac fate maps using a Gata4-based reporter of Cre activity. Dev. Biol. 323, 98–104 (2008).

[10] Laugwitz, K.-L. et al. Postnatal isl1+ cardioblasts enter fully differentiated cardiomyocyte lineages. Nature 433, 647–653 (2005).

[11] Moretti, A. et al. Multipotent embryonic isl1+ progenitor cells lead to cardiac, smooth muscle, and endothelial cell diversification. Cell 127, 1151–1165 (2006).

[12] Wu, S.M. et al. Developmental origin of a bipotential myocardial and smooth muscle cell precursor in the mammalian heart. Cell 127, 1137–1150 (2006).

[13] Mommersteeg, M.T.M. et al. Molecular pathway for the localized formation of the sinoatrial node. Circ. Res. 100, 354–362 (2007).

[14] Wiese, C. et al. Circ. Res. 104, 388–397 (2009).

[15] Liang, X. et al. HCN4 dynamically marks the first heart field and conduction system precursors. Circ. Res. 113, 399–407 (2013).

[16] Später, D. et al. A HCN4+ cardiomyogenic progenitor derived from the first heart field and human pluripotent stem cells. Nat. Cell Biol. 15, 1098–1106 (2013).

[17] Kattman, S.J. et al. Stage-specific optimization of activin/nodal and BMP signaling promotes cardiac differentiation of mouse and human pluripotent stem cell lines. Cell Stem Cell 8, 228–240 (2011).

[18] Wierstra, I. & Alves, J. The c-myc promoter: still mysterY and challenge. Adv. Cancer Res. 99, 113–333 (2008).

[19] Gittenberger-De Groot, A.C. et al. Nkx2.5 negative myocardium of the posterior heart field and its correlation with podoplanin expression in cells from the developing cardiac pacemaking and conduction system. Anat. Rec. 290, 115–122 (2007).

[20] Dyer, L.A. et al. BMP signaling modulates hedgehog-induced secondary heart field proliferation. Dev. Biol. 348, 167–176 (2010).

[21] Gude, N. et al. Akt promotes increased cardiomyocyte cycling and expansion of the cardiac progenitor cell population. Circ. Res. 99, 381–388 (2006).

[22] Keren-Politansky, A., Keren, A. & Bengal, E. Neural ectoderm-secreted FGF initiates the expression of Nkx2.5 in cardiac progenitors via a p38 MAPK/CREB pathway. Dev. Biol. 335, 374–384 (2009).

[23] Liberatore, C.M., Searcy-Schrick, R.D., Vincent, E.B. & Yutzey, K.E. Nkx-2.5 gene induction in mice is mediated by a Smad consensus regulatory region. Dev. Biol. 244, 243–256 (2002).

[24] Reifers, F., Walsh, E.C., Leger, S., Stainier, D.Y. & Brand, M. Induction and differentiation of the zebrafish heart requires fibroblast growth factor 8 (fgf8/acerebellar). Development 127, 225–235 (2000).

[25] Schultheiss, T.M., Burch, J.B. & Lassar, A.B. A role for bone morphogenetic proteins in the induction of cardiac myogenesis. Genes Dev. 11, 451–462 (1997).

[26] Barron, M., Gao, M. & Lough, J. Requirement for BMP and FGF signaling during cardiogenic induction in non-precardiac mesoderm is specific, transient, and cooperative. Dev. Dyn. 218, 383–393 (2000).

[27] Inman, G.J. et al. SB-431542 is a potent and specific inhibitor of transforming growth factor-β superfamily type I activin receptor-like kinase (ALK) receptors ALK4, ALK5, and ALK7. Mol. Pharmacol. 62, 65–74 (2002).

[28] Den Hartogh, S.C. et al. Dual reporter MESP1mCherry/w-NKX2–5eGFP/w hESCs enable studying early human cardiac differentiation. Stem Cells 33, 56–67 (2015).

[29] Yang, L. et al. Human cardiovascular progenitor cells develop from a KDR+ embryonic-stem-cell-derived population. Nature 453, 524–528 (2008).

[30] Ardehali, R. et al. Prospective isolation of human embryonic stem cell-derived cardiovascular progenitors that integrate into human fetal heart tissue. Proc. Natl. Acad. Sci. USA 110, 3405–3410 (2013).

[31] van Berlo, J.H. et al. c-kit+ cells minimally contribute cardiomyocytes to the heart. Nature 509, 337–341 (2014).

[32] James, D. et al. Expansion and maintenance of human embryonic stem cell-derived endothelial cells by TGFβ inhibition is Id1 dependent. Nat. Biotechnol. 28, 161–166 (2010).

[33] Marques, S.R., Lee, Y., Poss, K.D. & Yelon, D. Reiterative roles for FGF signaling in the establishment of size and proportion of the zebrafish heart. Dev. Biol. 321, 397–406 (2008).

[34] de Pater, E. et al. Bmp signaling exerts opposite effects on cardiac differentiation. Circ. Res. 110, 578–587 (2012).

[35] Ueno, S. et al. Biphasic role for Wnt/β-catenin signaling in cardiac specification in zebrafish and embryonic stem cells. Proc. Natl. Acad. Sci. USA 104, 9685–9690 (2007).

[36] Goumans, M.-J. et al. TGF-β1 induces efficient differentiation of human cardiomyocyte progenitor cells into functional cardiomyocytes in vitro. Stem Cell Res. 1, 138–149 (2007).

[37] Verkerk, A.O., van Ginneken, A.C.G. & Wilders, R. Pacemaker activity of the human sinoatrial node: role of the hyperpolarization-activated current, I(f). Int. J. Cardiol. 132, 318–336 (2009).

[38] Xi, J. et al. Comparison of contractile behavior of native murine ventricular tissue and cardiomyocytes derived from embryonic or induced pluripotent stem cells. FASEB J. 24, 2739–2751 (2010).

[39] Jackson, T. et al. The c-myc proto-oncogene regulates cardiac development in transgenic mice. Mol. Cell. Biol. 10, 3709–3716 (1990).

[40] Noseda, M., Peterkin, T., Simões, F.C., Patient, R. & Schneider, M.D. Cardiopoietic factors extracellular signals for cardiac lineage commitment. Circ. Res. 108, 129–152 (2011).

[41] Cai, W. et al. Coordinate Nodal and BMP inhibition directs Baf60c-dependent cardiomyocyte commitment. Genes Dev. 27, 2332–2344 (2013).

[42] Waldo, K.L. et al. Conotruncal myocardium arises from a secondary heart field. Development 128, 3179–3188 (2001).

[43] Milgrom-Hoffman, M. et al. The heart endocardium is derived from vascular endothelial progenitors. Development 138, 4777–4787 (2011).

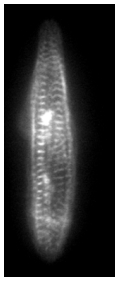

[44] Zhang, Q. et al. Direct differentiation of atrial and ventricular myocytes from human embryonic stem cells by alternating retinoid signals. Cell Res. 21, 579–587 (2011).

[45] Devalla, H.D. et al. Atrial-like cardiomyocytes from human pluripotent stem cells are a robust preclinical model for assessing atrial-selective pharmacology. EMBO Mol. Med. 7, 394–410 (2015).

[46] Kattman, S.J., Huber, T.L. & Keller, G.M. Multipotent Flk-1+ cardiovascular progenitor cells give rise to the cardiomyocyte, endothelial, and vascular smooth muscle lineages. Dev. Cell 11, 723–732 (2006).

[47] Qyang, Y. et al. The renewal and differentiation of Isl1+ cardiovascular progenitors are controlled by a WNT/β-catenin pathway. Cell Stem Cell 1, 165–179 (2007).

[48] Bu, L. et al. Human ISL1 heart progenitors generate diverse multipotent cardiovascular cell lineages. Nature 460, 113–117 (2009).

[49] Domian, I.J. et al. Generation of functional ventricular heart muscle from mouse ventricular progenitor cells. Science 326, 426–429 (2009).

[50] Moretti, A. et al. Mouse and human induced pluripotent stem cells as a source for multipotent Isl1+ cardiovascular progenitors. FASEB J. 24, 700–711 (2010).

[51] Elliott, D.A. et al. NKX2–5eGFP/w hESCs for isolation of human cardiac progenitors and cardiomyocytes. Nat. Methods 8, 1037–1040 (2011).

[52] Miano, J.M., Cserjesi, P., Ligon, K.L., Periasamy, M. & Olson, E.N. Smooth muscle myosin heavy chain exclusively marks the smooth muscle lineage during mouse embryogenesis. Circ. Res. 75, 803–812 (1994).